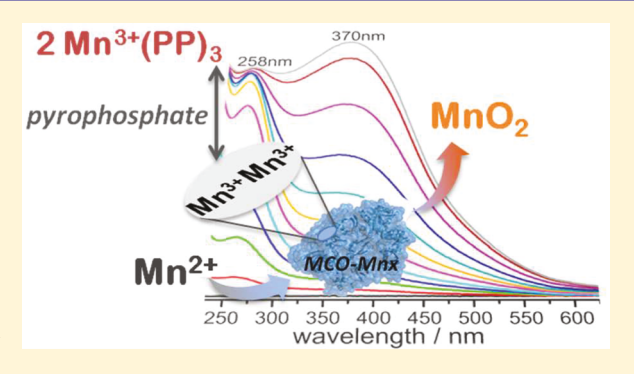


Mn(II) Oxidation by the Multicopper Oxidase Complex Mnx: A Coordinated Two-Stage Mn(II)/(III) and Mn(III)/(IV) Mechanism

Alexandra V. Soldatova, [†] Christine A. Romano, ^{§,‡} Lizhi Tao, ^{#,‡} Troy A. Stich, [#] William H. Casey, ^{#,⊥} R. David Britt, [#] Bradley M. Tebo, [§] and Thomas G. Spiro*, [†]

Supporting Information

ABSTRACT: The bacterial manganese oxidase MnxG of the Mnx protein complex is unique among multicopper oxidases (MCOs) in carrying out a two-electron metal oxidation, converting Mn(II) to MnO_2 nanoparticles. The reaction occurs in two stages: $Mn(II) \rightarrow$ Mn(III) and $Mn(III) \rightarrow MnO_2$. In a companion study, we show that the electron transfer from Mn(II) to the low-potential type 1 Cu of MnxG requires an activation step, likely forming a hydroxide bridge at a dinuclear Mn(II) site. Here we study the second oxidation step, using pyrophosphate (PP) as a Mn(III) trap. PP chelates Mn(III) produced by the enzyme and subsequently allows it to become a substrate for the second stage of the reaction. EPR spectroscopy confirms the presence of Mn(III) bound to the



enzyme. The Mn(III) oxidation step does not involve direct electron transfer to the enzyme from Mn(III), which is shown by kinetic measurements to be excluded from the Mn(II) binding site. Instead, Mn(III) is proposed to disproportionate at an adjacent polynuclear site, thereby allowing indirect oxidation to Mn(IV) and recycling of Mn(II). PP plays a multifaceted role, slowing the reaction by complexing both Mn(II) and Mn(III) in solution, and also inhibiting catalysis, likely through binding at or near the active site. An overall mechanism for Mnx-catalyzed MnO₂ production from Mn(II) is presented.

■ INTRODUCTION

Multicopper oxidases (MCOs) are widespread in nature and oxidize a variety of substrates, both organic and inorganic. 1,2 They contain a trinuclear Cu center for O2 reduction and a solitary Cu (type 1) adjacent to the substrate site. The type 1 Cu²⁺ extracts an electron from the substrate and transfers it to the trinuclear Cu site. Four successively transferred electrons reduce the O2 to H2O.3 The type 1 Cu is held trigonally by a cysteinate and two histidine ligands, with a weak or absent axial ligand. A wide range of type 1 Cu reduction potentials is found among the MCOs, allowing reaction with a wide range of reducing substrates.

The conversion of Mn(II) to MnO2 by bacterial MCOs represents a marked departure from this pattern. The reaction involves a two-electron metal oxidation, and extracting an electron from either Mn(II) or Mn(III) is energetically difficult. Moreover, no other class of MCOs has a biomineral as a final product. Unlike other MCOs, MnxG from marine Bacillus sp. PL-12⁹ (the only MCO to have been successfully expressed and purified, for which Mn(II) is thought to be the primary substrate 10) is tightly bound to small accessory proteins, MnxE and MnxF. This protein complex, Mnx, has been characterized, 10-13 and, surprisingly, the type 1 Cu reduction potential of MnxG was found to be at the low end of the MCO range, 0.38 V (vs Normal Hydrogen Electrode, pH 7.8). Indeed, the type 1 Cu²⁺ is not reduced by Mn(II) in the absence of O₂. Thus, MnxG does not work by matching its potential to that of its substrate.

Instead a different strategy is employed. MnxG exploits the polynuclear chemistry of manganese to adjust the Mn(III)/ Mn(II) reduction potential and facilitate MnO₂ formation. As detailed in the accompanying paper,8 the enzyme requires an activation step, likely involving deprotonation of Mn(II)-bound H₂O and bridging of the resulting hydroxide to a second Mn(II), thereby lowering the Mn(III)/Mn(II) reduction potential for efficient electron transfer. Turnover of this binuclear complex was proposed to produce a doubly hydroxide-bridged binuclear Mn(III) intermediate, Mn(III)(μ-OH)₂Mn(III). In this work, we present kinetic evidence for this intermediate, through Mn(III) trapping by pyrophosphate (PP). Moreover, we establish that Mn(III) cannot transfer an

Received: March 22, 2017 Published: July 17, 2017

Department of Chemistry, University of Washington, Box 351700, Seattle, Washington 98195, United States

[§]Division of Environmental and Biomolecular Systems, Institute of Environmental Health, Oregon Health & Science University, Portland, Oregon 97239, United States

[#]Department of Chemistry and [⊥]Earth and Planetary Sciences Department, University of California, Davis, One Shields Avenue, Davis, California 95616, United States

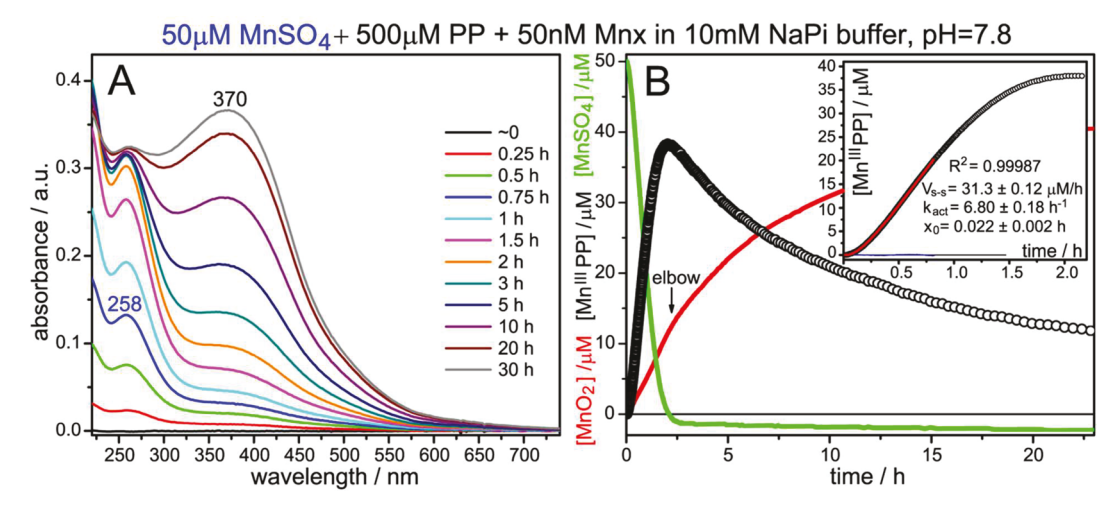


Figure 1. (A) UV—vis spectra taken at the indicated times during oxidation of 50 μ M MnSO₄ catalyzed by 50 nM Mnx, in the presence of 500 μ M NaPP in 10 mM NaPi buffer, pH 7.8. The 258 nm band represents the formation of the Mn(III) intermediate trapped by pyrophosphate; the band at ~370 nm is due to formation of nanoparticulate Mn oxides. (B) Concentration time courses for Mn(III)PP (black points), MnO₂ (red line), and Mn(II) (green line), obtained after absorption spectral data in (A) were converted to concentrations (see Methods and SI for details). The time courses show that Mn(III) is produced faster than MnO₂ but MnO₂ production directly from Mn(II) is faster than its production from the released Mn(III), evidenced by the elbow in the curve at the point where Mn(II) is depleted. *Inset*: Early portion of the Mn(III)PP time profile (black points) during the first 2.2 h, fitted to the activation equation, eq 1. The optimized parameters from the fit are indicated, together with the residual from the fit (blue line).

electron directly to the type 1 Cu. Instead we propose indirect Mn(III) oxidation via disproportionation in the binuclear, or a subsequent tetranuclear Mn(III) intermediate, with recycling of Mn(II) to the electron-transfer site. This mechanism is proposed to produce Mn(IV)(μ -O)₂Mn(IV), or an oligomer, as the primary enzyme product, which subsequently condenses to MnO₂ nanoparticles. Thus, MnxG facilitates two-step manganese oxidation via hydroxide and oxide bridging in successive polynuclear complexes. Analogous polynuclear Mn complexes are found in the O₂-evolving complex of photosystem II^{14–17} and in manganese catalase. ^{18–21}

METHODS

Methodology for monitoring reaction time courses via UV—vis absorption spectroscopy is described in the companion paper. Briefly, time-resolved spectra were recorded in a 10 mm path length cuvette with a Teflon stir bar using an Agilent (Santa Clara, CA, USA) 8453 UV—vis spectrophotometer with a thermostatable multicell transport configuration and an automated kinetic scan capability and paired with the Spinette magnetic stirring system (Starna Cells, Atascadero, CA, USA). Typically, five reaction assays were monitored in a parallel configuration.

Expression and purification of the Mnx enzyme complex were described previously. 9,10 In the companion paper, 8 we employed HEPES buffer, as in all previous studies, 9,10,22,23 but found it necessary to monitor the enzymatic reaction under the spectrophotometer's visible lamp only, to avoid interference from HEPES-induced photoreactions. In the present study, the UV lamp was required to monitor evolution of the 258 nm band of the Mn(III) intermediate trapped by pyrophosphate. To avoid photoreduction, we switched from HEPES to sodium phosphate (NaPi) buffer, buffer-exchanging the enzyme stock, which had been stored in HEPES, as well. (Several reports in the literature warn about Mn(III) pyrophosphate instability in HEPES buffer. 24,25 We confirmed that HEPES reduction of Mn(III) pyrophosphate correlated with the extent of the UV light exposure, and with concentration of HEPES, see Figure S1.) Assays (1 mL volume total) contained 50 nM Mnx in 10 mM sodium phosphate buffer at pH 7.8. MnSO₄ stock (prepared by dissolving MnSO₄·6H₂O (Sigma-Aldrich) in water) was at a concentration of 0.01 M. To prepare pyrophosphate stock solution, usually at 0.05 M, the

appropriate amount of sodium pyrophosphate tetrabasic (Sigma-Aldrich) was dissolved in water, and the pH was adjusted to \sim 7.8 by a dropwise addition of 1 N HCl. Mn(III) pyrophosphate stock was prepared by dissolving Mn(III) acetate (Sigma-Aldrich) in 0.05 M PP to yield 0.01 M Mn(III)PP₃.

For the UV-vis absorption measurements, the reaction was initiated by adding appropriate amounts of 0.01 M MnSO₄ or Mn(III) stocks to Mnx in NaPi buffer, having specified amounts of PP, directly into the cuvette. The absorbance in the 220-1000 nm region was measured over time every 30-60 s, increasing the acquisition time by 2-5% after 1 h, until the absorbance of the colloidal MnO₂ product (~370 nm) reached a plateau. In the absence of PP in the reaction assays,8 the MnO2 band shifted to longer wavelengths while growing, indicating that particle growth overlaps with the enzymatic reaction. Multivariate analysis was used to separate these processes.⁸ However, PP slows the enzymatic reaction considerably, giving the MnO₂ product time to age as it is produced. Minimal red-shift is observed, and multivariate analysis is unnecessary. To process the UV-vis timedependent absorption data, the data were background corrected, and the spectrum before the addition of Mn-substrate was subtracted. The time courses were extracted directly from the peak absorbance. The absorbance asymptote at the end of the reaction was used to determine the molar absorptivity of the MnO2 product (scattering due to colloidal nature of MnO2 is minimal <600 nm, in the region of the monitored enzymatic reaction), 26,27 and to calculate [Mn(III)PP] at earlier times (see SI). The Mn(III)PP molar absorptivity, $\varepsilon_{258 \text{ nm}}$ = 6100 M⁻¹cm⁻¹, was determined from stock solution dilutions.

Electron paramagnetic resonance (EPR) spectroscopic measurements were performed as described in Tao et al. ¹² Briefly, X-band continuous-wave (CW) EPR spectra were recorded using a Bruker (Billerica, MA) EleXsys E500 spectrometer. Cryogenic temperatures were achieved and controlled using an ESR900 liquid helium cryostat in conjunction with a temperature controller (Oxford Instruments ITC503) and gas flow controller. Additionally, for perpendicular-mode EPR ($B_0\bot B_1$), a superhigh Q resonator (ER4122SHQE) was employed, while all parallel-mode EPR experiments ($B_0 \parallel B_1$) made use of a dual-mode resonator (ER4116DM). All CW-EPR data were collected under slow-passage, nonsaturating conditions. Spectrometer settings were as follows: conversion time = 40 ms, modulation amplitude = 0.8 mT, and modulation frequency = 100 kHz.

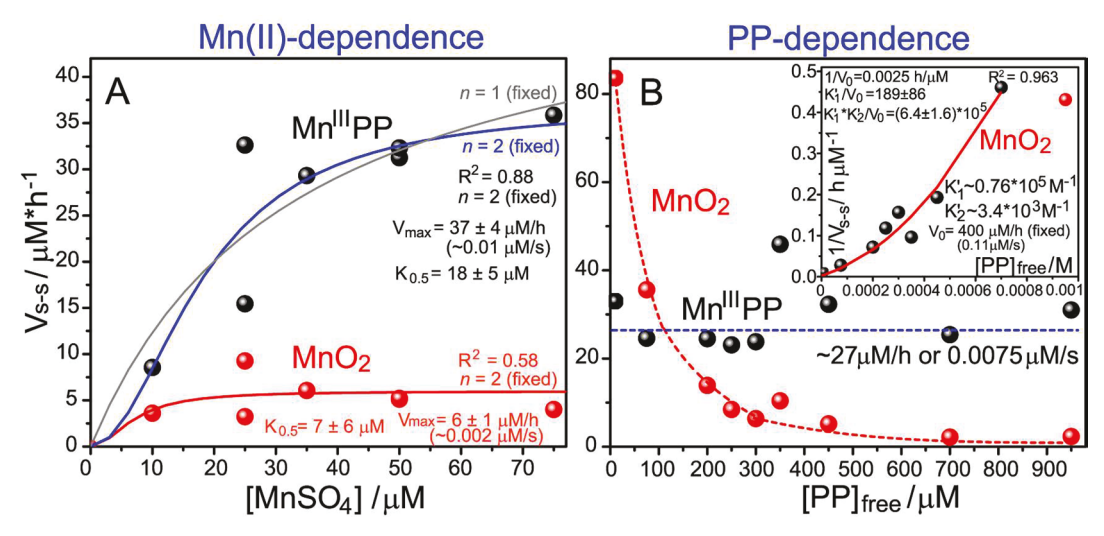


Figure 2. Dependence of the steady-state rate for 50 nM Mnx in NaPi buffer, pH 7.8, on (A) the starting Mn(II) concentration, in the presence of 500 µM NaPP and (B) the PP concentration with 50 µM Mn(II) starting concentration. See text for discussion of fitting parameters. (A) The steady-state rate dependencies for Mn(III) (black points) and MnO₂ (red points) productions are fit to the Hill equation³³ up to 75 µM MnSO₄, beyond which the apparent rates increase erratically due to abiotic reduction of MnO₂ by Mn(II) (Figure S9A). The blue and red lines are fits of Mn(III)PP and MnO₂ dependencies, respectively, fixing the Hill coefficient n at 2, with the indicated parameters, while the gray line is a fit of Mn(III)PP dependence produced by fixing n at 1 (r = 0.86). (B) The steady-state rate of Mn(III)PP production (black points) is independent of [PP], while the steady-state rate of MnO2 production (red points) declines hyperbolically. Inset: Fitting the MnO2 steady-state rate dependence of PP with eq 3 gives the conditional formation constants K'_1 and K'_2 (see text); the red point at the highest [PP] was excluded from the fit.

RESULTS AND DISCUSSION

1. Pyrophosphate Reveals Mn(III) as an Intermediate on the Path to MnO₂. As has previously been reported, adding pyrophosphate (PP) when Mn(II) is oxidized by Mnx reveals production of Mn(III) as an intermediate, detectable via the growth of a 258 nm absorption band, characteristic of a Mn(III)PP complex, which subsequently disappears. It is replaced by the ~370 nm absorption band due to colloidal MnO₂, the final product (Figure 1A). MnO₂ production is much slower (hours instead of minutes) than without PP, for several reasons, as discussed below. The MnO2 absorption band does not shift as it grows (in contrast to its behavior in the absence of PP8), indicating that the enzyme reaction has become slower than the nanoparticle aging process. Consequently, the growth rate of the MnO₂ band now reflects the retarded rate of the enzyme reaction directly.

As in the kinetic assays without PP,8 millimolar concentrations of NaCl in the buffer were found to precipitate the colloidal MnO2, precluding quantitative analysis. Salts were therefore omitted from the assays. In addition, we switched from HEPES to phosphate buffer, because Mn(III)PP is photoreduced in the presence of HEPES (see Figure S1 and ref 24, 25, 28-31 for other examples of HEPES as a metal reductant).

Concentration-time profiles (Figure 1B), obtained after converting absorbances to concentrations (Methods and SI), show that MnO₂ is produced from the beginning, though more slowly than Mn(III)PP, and that its profile exhibits an elbow, where the initial rate changes to a still slower one. The elbow occurs when Mn(II) (calculated from the Mn mass balance; green line in Figure 1B and in Figures S2 and S6) is exhausted, and the only reactant left is Mn(III). Thus, formation of MnO₂ directly from Mn(II) is faster than it is from Mn(III) in solution. We conclude that Mn(III) is an enzymatic intermediate that can be extracted and re-inserted by PP in solution.

Analysis of the concentration profiles is complicated by a competing abiotic reduction of MnO₂ by Mn(II) that produces Mn(III)PP. This reaction diminishes [MnO₂] and enhances [Mn(III)] production relative to the enzyme profiles. Control experiments with synthetic MnO₂ colloids (Figure S11) indicate that this reaction is slower than the enzymatic reaction, but does occur on the same time scale (Figure S12). However, the rate is proportional to the [Mn(II)][MnO₂] concentration product, and is therefore insignificant early in the reaction, when [MnO₂] is low. We therefore limit our analysis to this

2. Mnx Kinetics Show That PP Does Not Alter the **Enzyme Mechanism.** The data reveal that PP does not alter the enzyme mechanism. The Mn(III)PP profile (Figure 1B, inset) is sigmoidal, as was the MnO2 profile in the absence of PP, and similar lag, activation, and turnover phases are evident. Moreover, turnover for Mn(III)PP is cooperative with respect to Mn(II) concentration (see below), as it was for MnO₂ without PP.8 The Mn(III) production time courses can be fit (Figure 1B, inset and Figures S3 and S7) to the kinetic equation for enzymes requiring activation,³²

[Mn(III)PP] =
$$V_{s-s}(x - x_0) - \frac{V_{s-s}}{k_{act}} (1 - e^{-k_{act}(x - x_0)})$$
 (1)

yielding activation rate constant, k_{act} , and catalytic turnover (steady-state) rate, $V_{\text{s-s}}$. There is also a lag time prior to Mn(III)PP detection, x_0 , whose magnitude was obtained from the fit. These parameters were determined over a range of Mn(II) (Figure S7) and PP (Figure S3) concentrations. The MnO₂ production time courses are more complex (Figure 1B and Figures S4 and S8), reflecting additional contributions associated with Mn(III) release and recapture. However, steady-state rates could be determined from their linear

The steady-state rate dependencies are shown in Figure 2. The steady-state rates for both Mn(III) and Mn(IV)

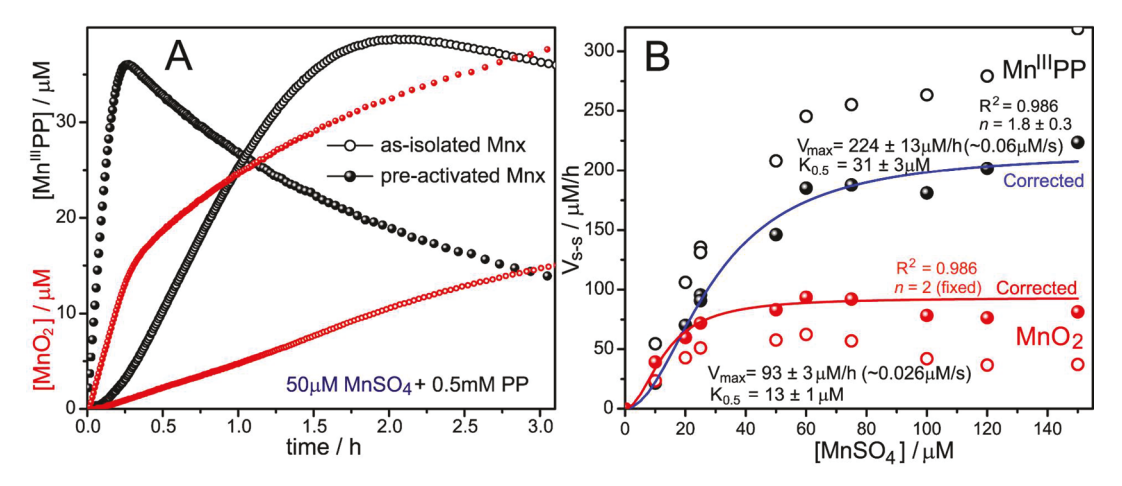


Figure 3. (A) Pre-activation of Mnx by 10 µM MnSO₄ turnover eliminates the activation step during subsequent Mn(II) oxidation cycles: Time course comparison for Mn(III)PP (black symbols) and MnO₂ (red symbols) production during oxidation of 50 μ M Mn(II) in 0.5 mM NaPP (10 mM NaPi buffer, pH 7.8) by as-isolated (open circles) and pre-activated (closed circles) 50 nM Mnx. (For pre-activated enzyme, the time points were obtained after subtraction of the background absorption from the 10 µM MnO₂ produced during pre-activation, see Figure S13.) (B) Mn(II)concentration dependence of the steady-state rates of initial Mn(III)PP (black circles) and MnO₂ productions (red circles) obtained using Mnx preactivated by 10 μ M Mn(II) turnover. These values were corrected for the abiotic contribution (see text for details), and replotted (black and red points for Mn(III)PP and MnO_2 production, respectively). Fits to Hill's equation for Mn(III)PP (blue line) and MnO_2 (red line, fixing n at 2) data

productions in PP reveal cooperative dependence on starting Mn(II) concentration (Figure 2A), just as the steady-state rate does for Mn(IV) in the absence of PP. In both cases the curves follow a Hill equation (fixing n at 2), implying cooperative uptake of two Mn(II) ions. The data are somewhat scattered for as-isolated Mnx (Figure 2A), reflecting uncertainties associated with the time-course fitting. However, cooperativity is evident.

More reliable data were obtained with pre-activated Mnx, produced by incubating the as-isolated enzyme with a small amount (0.01 mM) of Mn(II), without PP (see Figure S13). Subsequent additions of Mn(II) in 0.5 mM PP produced hyperbolic time courses of product without the complication of lag or activation phases (Figure 3A and Figures S14), and the turnover rates were obtained from the initial, linear portions for both, Mn(III)PP and MnO₂ production curves (Figures S15). However, because 10 µM MnO₂ was present at the start of the reaction, the contribution of its abiotic reduction by Mn(II) had to be considered in analyzing these rates. We estimated this contribution with synthetic MnO₂ colloids, ^{34,35} by monitoring the abiotic reaction of 10 µM synthetic MnO2 with varying amounts of Mn(II) in the presence of 0.5 mM PP via the Mn(III) and MnO₂ absorption bands (Figure S11). The Mn(III) production and MnO₂ decay rates were determined from the initial time courses (Figure S12), and used to correct the enzymatic rates at each starting [Mn(II)], taking into account that the abiotic reaction consumes one MnO2 and produces two Mn(III) per Mn(II) reacted (Figure 3B). The abiotic corrections are modest, and do not affect the shape of the curves, which are clearly sigmoidal for both Mn(III) and MnO_2 , and give a more satisfactory fit with n = 1.8, close to the value determined in the absence of PP.8 This agreement, with and without PP, is a strong evidence that PP does not alter the enzyme mechanism, which involves turnover of a dinuclear hydroxide-bridged Mn(II) complex, after enzyme activation.⁸

3. EPR Spectroscopy Detects Mn(III) on the Enzyme. Mn(II)-substrate binding to Mnx was characterized previously by EPR, 12 but no signals from oxidized Mn were detected.

However, in the presence of PP, we obtained EPR evidence (Figure 4B, spectrum g) for Mnx-bound Mn(III) under turnover conditions (0.4 mM Mn(II) added to 0.1 mM Mnx in 0.5 mM PP, under O2 exposure, and flash-frozen after 3 min). The spectrum contains sextet of hyperfine signals, with a $g_{\rm eff} = 8.13$ (centered at 82.0 mT magnetic field) and a 55 Mn hyperfine coupling parameter (A = 42 G, corresponding to 120 MHz), attributable to mononuclear Mn(III), and differs significantly from that of Mn(III) in PP solution 36-38 (Figure 4B, spectrum e, A = 48 G). This is the first spectroscopic evidence confirming enzyme-bound Mn(III) as an intermediate in the oxidation of Mn(II).

The kinetic evidence (see below) favors binuclear Mn(III)- $(\mu$ -OH)₂Mn(III) as the enzyme intermediate; the EPR spectrum of this integer spin system would be broad, and likely not observable at these low concentrations. However, when $Mn(III)(\mu$ -OH)₂Mn(III) is produced transiently from Mn(II), it could lose some of its Mn(III) via PP trapping, leaving behind enough mononuclear Mn(III) to produce the EPR signal observed in the freeze-quench experiment. Without PP, this signal is not observed, since very little Mn(III) dissociates from the enzyme. Moreover, it is not observed when Mn(III)PP is added to Mnx (Figure 4B, spectrum f), likely because Mn(III) binds bimolecularly (see below), as the unobservable Mn(III)(μ -OH)₂Mn(III).

In the absence of O2, EPR spectroscopy revealed the same Mnx-bound Mn(II) signals we saw in the absence of PP, from both mononuclear (class ii, Figure 4A), 39,40 and weakly coupled dinuclear Mn(II) (class iii, Figure 4A). 12,41-43 No spectral changes are observed in the CW EPR spectrum obtained in the presence of PP, perhaps indicating that the electronic structure of bound Mn(II) in Mnx is not altered, despite the kinetic evidence (see below) that PP reduces the Mn(II) off rate. However, we note Mn(II) sites with zero-field splittings of D >1000 MHz give rise to broad CW EPR signals that may not be visible among all the other Mn(II) signals in these spectra. The Mn(II) signal in PP solution (absent Mnx) consists of the classical six-line signal seen for $Mn(H_2O)_6^{2+39}$ but with

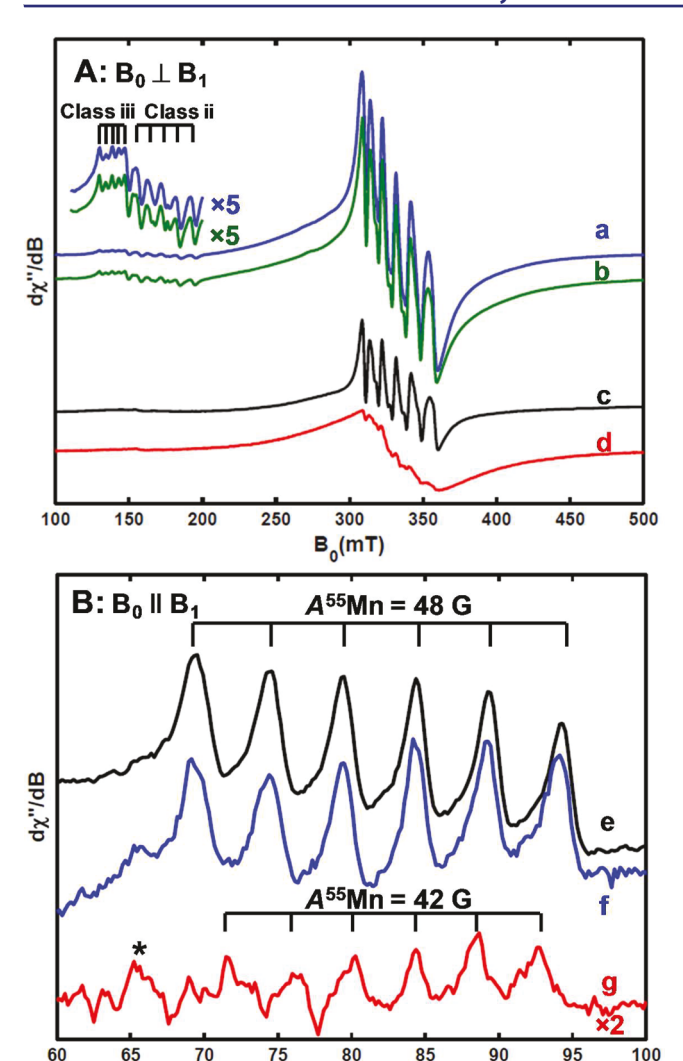


Figure 4. (A) X-band perpendicular-mode CW EPR spectra of (a) 260 μM fully reduced Mnx protein complex that was anaerobically incubated with 0.8 equiv Mn(II); (b) 200 µM fully reduced Mnx protein that was anaerobically incubated with 1 equiv Mn(II) in the presence of 5 equiv PP; (c) $100 \mu M \text{ Mm}^{2+}$ aqueous solution; (d) 100μM Mn(II) with 1 equiv. PP in HEPES buffer solution (20 mM HEPES, 20 mM NaCl, pH 7.8, 20% ethylene glycol). Class ii and Class iii signals refer to the mononuclear bound Mn(II) and weakly coupled dinuclear Mn(II) in Mnx protein complex, respectively (see ref 12). Experimental parameters: temperature = 15 K; microwave frequency = 9.38 GHz; microwave power = 0.6325 mW; conversion time = 40 ms; modulation amplitude = 0.8 mT; modulation frequency = 100 kHz. (B) X-band parallel-mode CW EPR spectra of (e) 200 µM Mn(III)PP in HEPES buffer solution (20 mM HEPES, 20 mM NaCl, pH 7.8, 20% ethylene glycol); (f) 100 µM oxidized Mnx protein that was aerobically incubated with 2 equiv of Mn(III)PP and hand-quenched after 5 min; (g) 100 μ M Mnx protein in 0.5 mM PP, aerobically incubated with 4 equiv Mn(II), and hand-quenched after being allowed to react for 3 min. The starred peak is a signal from background. Experimental parameters: temperature = 8 K; microwave frequency = 9.38 GHz; microwave power = 10 mW; conversion time = 40 ms; modulation amplitude = 0.8 mT; modulation frequency = 100 kHz.

 $B_0(mT)$

significant broadening (Figure 4A, spectrum d), possibly due to the presence of Mn(II)PP aggregates. 44,45

4. Mn(II) Is Required for Mn(III) Oxidation. Mnx can also catalyze the oxidation of external Mn(III) in PP (Figure 5A and

Figure \$10), as reported previously. However, we found that conversion of Mn(III) to MnO2 is much slower starting with Mn(III) than with Mn(II) (Figure 5B), and is greatly accelerated by the presence of small amounts of Mn(II) (added as MnSO₄ stock to Mnx assays containing Mn(III)PP, Figure S18), Figure 5B, inset.

In the absence of added Mn(II), the reaction is slow and variable, being highly sensitive to the trace of Mn(II) present in the Mn(III) stock. Adding 5 μ M Mn(II) accelerates the reaction significantly, and 20 µM Mn(II) is sufficient to restore the rate to that seen when Mn(II) alone is the substrate. We infer that Mn(II) binding is a requirement for the further reaction of Mn(III). Furthermore, the presence of Mn(III) has no effect on Mn(II) oxidation. In the presence of Mn(III), Mn(II) oxidation still produces sigmoidal Mn(III) production curves, with the expected dependencies of the rate parameters (Figure S18). Thus, Mn(III) does not compete with Mn(II) for binding to the enzyme.

5. Mn(IV) Is Produced by Disproportionation of Mn(III) via a Dinuclear Complex, with Recycling of Mn(II). If Mn(III) is excluded from the Mn(II) substrate site, then direct electron transfer from Mn(III) to the type 1 Cu²⁺ of MnxG is precluded. In that case, the only plausible route available for Mn(IV) formation is Mn(III) disproportionation to Mn(IV) and Mn(II), followed by recycling of Mn(II). The kinetic data provide clear evidence that Mn(IV) production does indeed involve Mn(II) recycling. The steady-state rate dependence on PP concentration (Figure 2B) reveals a striking difference between Mn(III) and Mn(IV) productions. The former is independent of [PP], implying that Mn(III) release from Mnx is rate limiting: PP does not attack the Mn(III) site, but is a passive trapping agent. In contrast, V_{s-s} for Mn(IV) production starts at a higher value and decreases hyperbolically with [PP]. If Mn(II) recycling after disproportionation is rate limiting for Mn(IV) production, then the rate would diminish with the free Mn(II) concentration resulting from PP chelation. This effect can be predicted from the mass balance:

$$C_{\text{Mn}} = [\text{Mn}] + [\text{Mn}(\text{II})\text{PP}] + [\text{Mn}(\text{II})(\text{PP})_2]$$

= $[\text{Mn}](1 + K_1'[\text{PP}] + K_1'K_2'[\text{PP}]^2)$ (2)

where C_{Mn} and [Mn] are the total and free Mn(II) concentrations, K'_1 and K'_2 are successive conditional formation constants for Mn(II)PP and Mn(II)(PP)₂ (both complexes have been reported in the literature 46) and [PP] is the concentration of uncomplexed pyrophosphate in its protonation state at the solution pH 7.8 (obtained by subtracting C_{Mn} from the analytical PP concentration to correct for PP bound as Mn(II)PP, the main complex in solution). The turnover rate is reduced by the ratio [Mn]/ $C_{\rm Mn}$, i.e., $V_{\rm s-s}$ = $V_0([\mathrm{Mn}]/C_{\mathrm{Mn}})$, or

$$V = V_0 \left[\frac{1}{1 + K_1'[PP] + K_1' K_2'[PP]^2} \right]$$
 (3)

where V_0 is the steady-state rate at zero PP.⁸ The inset in Figure 2B shows the fit, which gives $K'_1 = 0.8 \times 10^5 \text{ M}^{-1}$ and $K'_2 = 3.4$ \times 10³ M⁻¹. The conditional formation constants, K', can be converted to fundamental formation constants, K, by accounting for the fraction of pyrophosphate which is unprotonated. The relevant pK_a values⁴⁷ are 6.7 for H_2PP^2 , and 9.4 for HPP^{3-} , from which the PP^{4-} concentration is calculated to be 1/44 of the analytical pyrophosphate

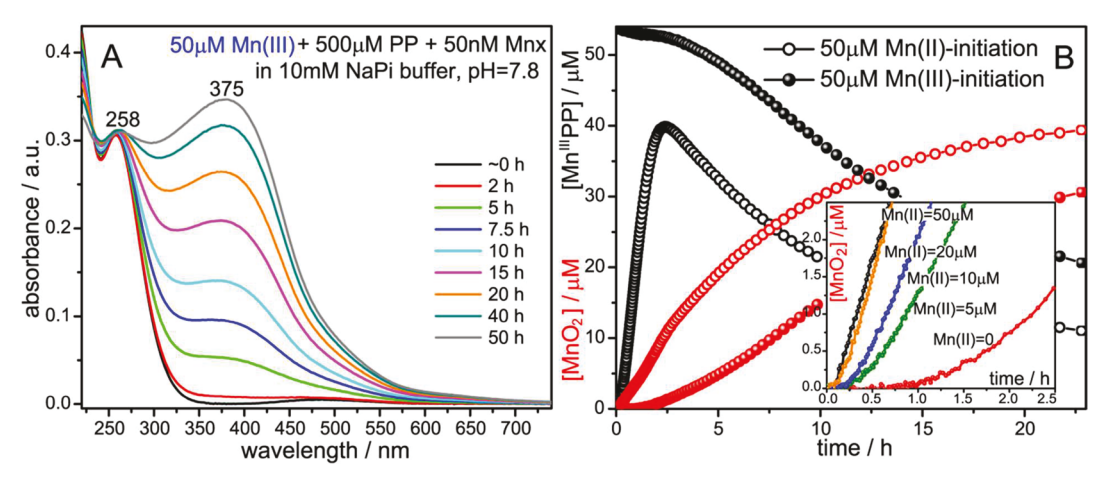


Figure 5. (A) UV—vis spectra taken at the indicated times during oxidation of 50 μ M Mn(III) acetate in PP catalyzed by 50 nM Mnx, in the presence of 500 μ M NaPP in 10 mM NaPi buffer, pH 7.8. The 258 nm band is due to Mn(III) substrate added as Mn(III)PP; the band at ~370 nm is due to formation of nanoparticulate Mn oxides. (B) Time courses for the Mn(III)PP and MnO₂ components obtained during oxidation of 50 μ M MnSO₄ (open circles) or 50 μ M Mn(III) (closed circles) by 50 nM Mnx in the presence of 500 μ M NaPP in 10 mM NaPi buffer, pH 7.8, extracted from the UV—vis time-resolved data using extinction coefficients obtained for the 250 μ M PP experiment from the [PP]-dependence series (see SI). Note the delay in the MnO₂ production in the case of Mn(III) substrate. *Inset*: MnO₂ traces during the first 2.5 h time, obtained when Mn(III)-initiation assay (red line) was spiked with 5 μ M MnSO₄ (green line), 10 μ M MnSO₄ (blue line), or 20 μ M MnSO₄ (orange line) (see also Figure S18). The 20 μ M MnSO₄ spike eliminated the delay in the MnO₂ production, resulting in the MnO₂ time trace that is almost superimposable with the trace from the 50 μ M Mn(II) initiation (black line).

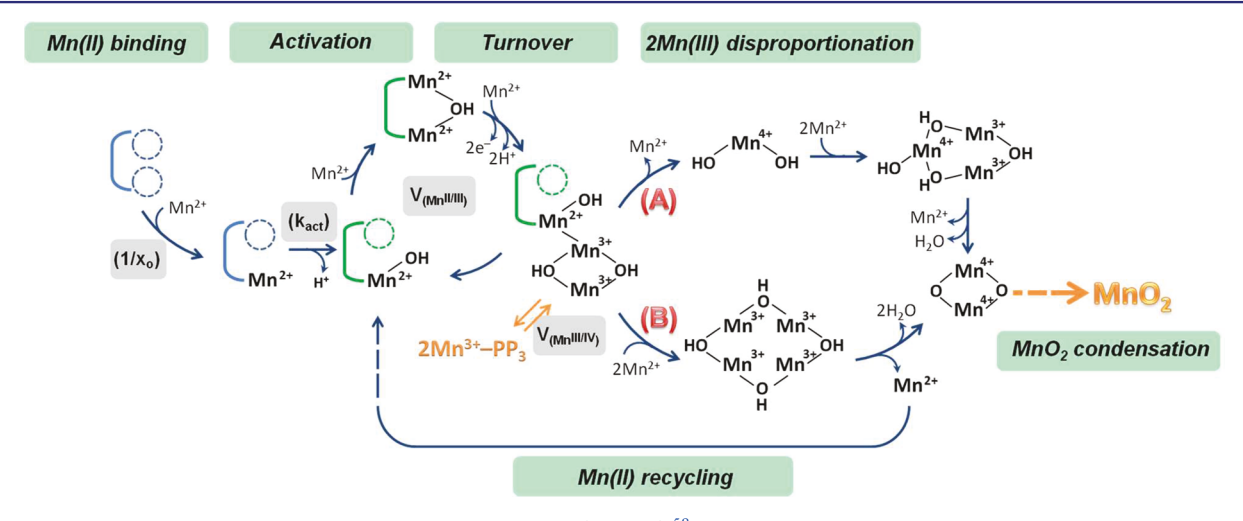


Figure 6. Proposed mechanism of Mnx-catalyzed MnO₂ formation (see text).⁵⁸

concentration. The fundamental formation constants are therefore 44K', giving $K_1 = 0.35 \times 10^7 \,\mathrm{M}^{-1}$ and $K_2 = 1.5 \times 10^5 \,\mathrm{M}^{-1}$. K_1 is in good agreement with the literature value of $10^7 \,\mathrm{M}^{-1}$. (No previous value of K_2 has been reported.) This agreement establishes that PP chelation of Mn(II) specifically inhibits Mn(IV) production, implying an essential role for Mn(II) recycling.

Disproportionation requires that at least two Mn(III) ions be adjacent in a polynuclear complex. In the accompanying article we reported evidence implicating a binuclear complex, Mn(III)(μ -OH)₂Mn(III) as the key intermediate in enzyme turnover. Below, we report further evidence in support of this inference, from the Mn(III) concentration dependence of the turnover rates for MnO₂ production from Mn(III) (Figure 9A). A clear second-order dependence was found. Thus, MnO₂ production requires simultaneous binding by two Mn(III) to the enzyme, implying that the Mn(III) reaction site is binuclear. The Mn(III)(μ -OH)₂Mn(III) provides a pathway for disproportionation via electron transfer between the Mn(III) ions:

$$Mn(III)(\mu\text{-OH})_2Mn(III) \rightarrow Mn(II) + Mn(IV)(OH)_2$$

The Mn(II) would be recycled and oxidized to Mn(III) by the enzyme, leaving Mn(IV)(OH)₂ as the next intermediate, awaiting condensation with additional Mn(IV)(OH)₂ units from subsequent enzyme turnovers. We had earlier argued that a mononuclear Mn(IV) intermediate is unlikely, since it would likely oxidize the protein side chains that are available as ligands. However, this possibility cannot be excluded *a priori*, since at least one instance of a mononuclear Mn(IV) protein complex has been reported, albeit without structural information. A second Mn(IV)(OH)₂ would condense with the first, forming binuclear Mn(IV)(μ -O)₂Mn(IV):

$$2Mn(IV)(OH)_2 \rightarrow Mn(IV)(\mu-O)_2Mn(IV) + 2H_2O$$

Alternatively, an easier disproportionation path would be available via a *tetranuclear* Mn(III) intermediate, which could be formed through two successive enzyme turnovers, via self-condensation of Mn(III)(μ -OH)₂Mn(III). A double dispro-

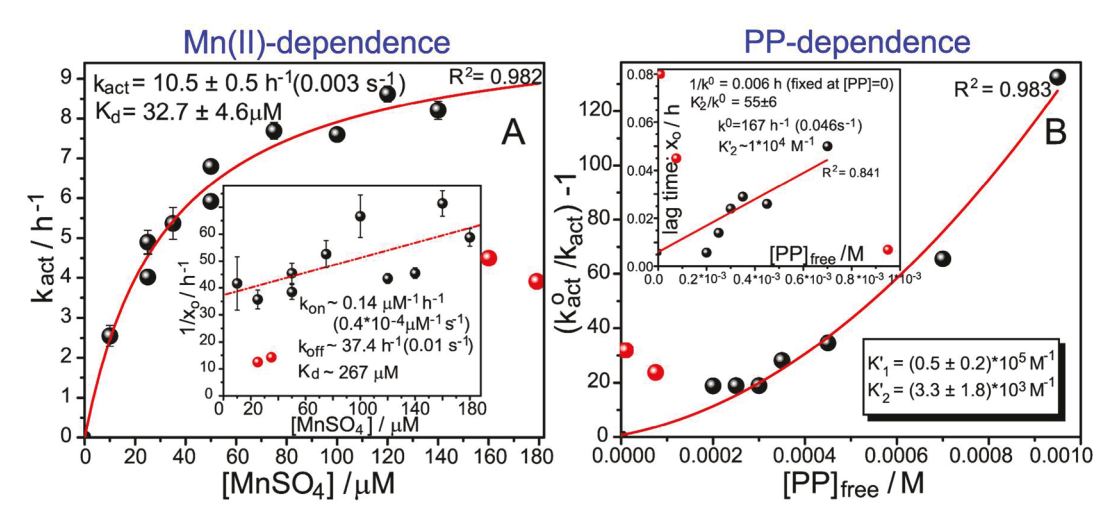


Figure 7. Dependence of activation equation parameters for 50 nM Mnx in NaPi buffer, pH 7.8, on (A) the starting Mn(II) concentration, in the presence of 0.5 mM NaPP, and (B) the PP concentration with 0.05 mM Mn(II) starting concentration. See text for discussion of fitting parameters. (A) The activation rate constant has a hyperbolic dependence on Mn(II) concentration, which can be fit to a binding model for the activation site. *Inset*: Dependence of the lag time (expressed as a rate) on Mn(II) concentration in the presence of 0.5 mM PP. The red line is the fit to a simple binding model, eq 4. (B) Fitting the activation rate constant dependence of PP with eq 8 gives the conditional formation constants K'_1 and K'_2 . *Inset* shows fitting result for the lag time dependence using the reciprocal of eq 5. The red points, corresponding to 60 and 125 μ M PP assays, do not follow the expected trend (probably due to inadequate suppression of Mn(III) disproportionation in solution or to aggregate formation at high [Mn(II)]:[PP] ratios), and were excluded from the fits.

portionation of two $Mn(III)(\mu-OH)_2Mn(III)$ could release two Mn(II) and produce binuclear $Mn(IV)(\mu-O)_2Mn(IV)$ directly:

$$\begin{split} &2Mn(III)(\mu\text{-OH})_2Mn(III) \\ &\rightarrow 2Mn(II) + 2H_2O + Mn(IV)(\mu\text{-O})_2Mn(IV) \end{split}$$

Oxo-bridging strongly stabilizes Mn(IV), and many oxo-bridged Mn(IV,IV) complexes are known. $^{14,50-54}$ We propose that Mn(IV)(μ -O)₂Mn(IV) or an oligomer is the enzyme product. It can condense with successively formed units into MnO₂, either at the enzyme active site, or after transfer to a distal nucleation site, either on the protein or in solution. The proposed formation mechanism of the ferritin's ferrihydrite-like core via migration of Fe(III)(μ -OH)₂Fe(III) units formed at the Fe(II) oxidation site SS,SO may offer an analogy, although MnO₂ grows outside of Mnx, and not in a cavity. SO

- **6. Overall Mechanism.** On the basis of these observations, together with those in the accompanying paper, we propose a full mechanism for MnO₂ production by Mnx, as diagrammed in Figure 6.
 - 1. Mn(II) binds weakly to as-isolated enzyme.
 - 2. Deprotonation of $Mn-OH_2$ at the Mnx substrate site activates the enzyme via a conformation change that enhances Mn(II) affinity.
 - 3. A second Mn(II) binds and bridges to the first, triggering electron transfer and Mn(II) translocation. Two cooperative turnovers produce Mn(III)(μ -OH)₂Mn(III), which
 - 4. proceeds to $Mn(IV)(\mu-O)_2Mn(IV)$ via
 - (A) disproportionation and condensation of successively produced $Mn(IV)(OH)_2$ units or
 - (B) condensation of successively produced $Mn(III)(\mu-OH)_2Mn(III)$ units followed by a double disproportionation. Pyrophosphate can trap Mn(III) and redeposit it at the binuclear Mn(III) site. Mn(II) is recycled to the substrate site.

- 5. $Mn(IV)(\mu-O)_2Mn(IV)$, the initial enzyme product, condenses further to MnO_2 nanoparticles, with release of two additional protons, four in total (since $2Mn(II) + O_2 + 2H_2O \rightarrow 2MnO_2 + 4H^+$). This process may occur near the substrate site and/or at a distal site. The role of the protein in controlling nanoparticle nucleation and growth remains to be determined.
- **7. Further Roles of PP.** 7.1. PP Inhibits Mnx Activation, while Also Competing with Mnx for Mn(II) Binding. The lag time, x_0 , obtained from fitting the Mn(III)PP time courses with the activation eq (Figures S3 and S7), is significantly longer than was observed in the absence of PP. For example, at $50 \mu M$ starting Mn(II) concentration, the lag time is ~ 90 s versus ~ 20 s for the assay without pyrophosphate. As in the absence of PP, 8 the reciprocal of the lag time, $1/x_0$, increases linearly with the starting [Mn(II)] (Figure 7A, inset), and is attributed to slow Mn(II) binding to as-isolated enzyme. The dependence can be fit to a simple binding model:

$$Mnx + Mn(II) \underset{k_{-1}}{\overset{k_1}{\rightleftharpoons}} Mnx - Mn(II)$$

$$1/x_0 = k_{\text{obs}} = k_1[Mn(II)] + k_{-1}$$
(4)

Although the data are scattered, and the parameter uncertainties are large, the parameters can nevertheless be compared qualitatively with those obtained in the absence of PP. The on rate is ~10 times lower (0.4 × 10⁻⁴ vs 4.4 × 10⁻⁴ μ M⁻¹ s⁻¹) and the off rate is ~3 times lower (0.010 vs 0.033 s⁻¹), giving a ~3.6 times higher dissociation constant (267 vs 75 μ M). A lower on rate is an expected consequence of Mn(II) complexation by PP. However, the conditional formation constant $K'_1 = 0.8 \times 10^5$ M⁻¹ (above) predicts a [Mn(II)]/[Mn(II)PP] ratio of 0.025 in 0.5 mM PP, far smaller than the observed ~10 times lowering of k_{on} . We infer that Mn(II) does not bind to Mnx as the free ion, but as Mn(II)PP. The ~10 times lowering of k_{on} reflects Mn(II)PP₂ formation, and/or slower binding of Mn(II)PP than free Mn(II).

The effect of Mn(II)PP2 can also be seen in the [PP] dependence of the binding rate (Figure 7B, inset and Figure S9B, inset). As discussed above for the Mn(IV) turnover dependency on PP, the chelation effect can be derived from the Mn(II) mass balance (eq 2), but in this case the binding rate is reduced by the ratio $[Mn(II)PP]/C_{Mn} = 1/(1 + K_2'[PP])$ (since $[Mn(II)] \ll [Mn(II)PP]$):

$$k_{\rm obs} = k^0 \left[\frac{1}{1 + K_2'[PP]} \right]$$
 (5)

where k^0 is the binding rate in the absence of PP. Although the data are scattered (reflecting uncertainties associated with time zero (mixing time) and aggregate formation at high [Mn(II)]: [PP] ratios), the best fit of the lag phase rates to the reciprocal of eq 5 (Figure 7B, inset) gives $K'_2 = 1 \times 10^4 \,\mathrm{M}^{-1}$, in reasonable agreement with the value determined from the Mn(IV) production rate $(3.4 \times 10^3 \text{ M}^{-1}, \text{ above})$. Thus, Mn(II) binds to as-isolated Mnx as Mn(II)PP complex.

PP chelation is also responsible for the hyperbolic decrease in the activation rate constant, k_{act} as the starting Mn(II) decreases (Figure 7A). A simple hyperbolic binding fit of the data gives $K_d = 33 \mu M$, in 0.5 mM PP, while in the absence of PP, k_{act} was found to be independent of starting [Mn(II)], implying that K_d < 10 μ M, the lowest Mn(II) concentration measured.8 Thus, PP also competes with the activation site for Mn(II) binding. The PP concentration dependence of k_{act} (Figure S9B and Figure 7B) can be fit assuming that the rate is proportional to the occupancy of the activation site,

$$k_{\text{act}}^{\text{PP}} = k_{\text{act}}^{0} \frac{[\text{EM}]}{[\text{E}] + [\text{EM}]}$$
(6)

where EM and E are metal-bound and unbound enzyme, with dissociation constant K_d . Then,

$$k_{\text{act}}^{\text{PP}} = k_{\text{act}}^{0} \frac{1}{1 + K_{\text{d}}/[\text{Mn}]}$$
 (7)

Once again, the effect of PP chelation on Mn(II) can be obtained from the mass balance (eq 2); substitution in eq 7 and rearranging gives

$$\frac{k_{\text{act}}^{\text{o}}}{k_{\text{act}}^{\text{PP}}} - 1 = \frac{K_{\text{d}}}{C_{\text{Mn}}} (1 + K_{1}'[\text{PP}] + K_{1}'K_{2}'[\text{PP}]^{2})$$
(8)

where $K_{\rm d}$ = 33 μ M, and the PP dependence was determined at $C_{\rm Mn}$ = 50 μ M. $k_{\rm act}^{\rm o}$ was measured in the absence of PP as ~0.06 s^{-1.8}

Using these values, the data were fit to eq 8 (Figure 7B) giving $K'_1 = 0.5 \times 10^5 \text{ M}^{-1}$ and $K'_2 = 3 \times 10^3 \text{ M}^{-1}$, in fair agreement with the values obtained from the Mn(IV) turnover rates. Thus, the activation kinetics are consistent with PP competition with Mnx for Mn(II) binding to the activation site.

In addition, PP clearly inhibits the activation step since at full site occupancy in 0.5 mM PP (Figure 7A), k_{act} is only 0.003 s⁻¹, 20-fold lower than in the absence of PP ($\sim 0.06 \text{ s}^{-1}$).8 Since asisolated Mnx binds PP along with Mn(II), we speculate that this PP inhibits activation by increasing the pK_a for the activation-inducing deprotonation of Mn(II)-OH2, perhaps by H-bonding to it. Alternatively, it may inhibit the accompanying conformation change, which increases the Mn(II) affinity of the

The 20-fold inhibition of the activation step in 0.5 mM PP carries forward to the catalytic step (Figure 2A): $V_{\text{max}} = 0.01$ μ M/s for Mn(III), and only 0.002 μ M/s for Mn(IV), whereas the overall $V_{\text{max}} = 0.20 \ \mu\text{M/s}$ in the absence of PP.⁸ The activation step is eliminated in pre-activated Mnx, and the rates are much higher (Figure 3B), 0.06 μ M/s for Mn(III), and 0.03 μ M/s for Mn(IV).

7.2. Mn(III) in PP Solution Exists as Mn(III)(PP)₃, and One PP Is Lost from Each of the Two Mn(III) That Bind to Mnx Together. Production of MnO2 is quantitative at PP concentrations up to 250 μ M, but the yields diminish progressively at higher PP concentrations (Figure 8 and Figure

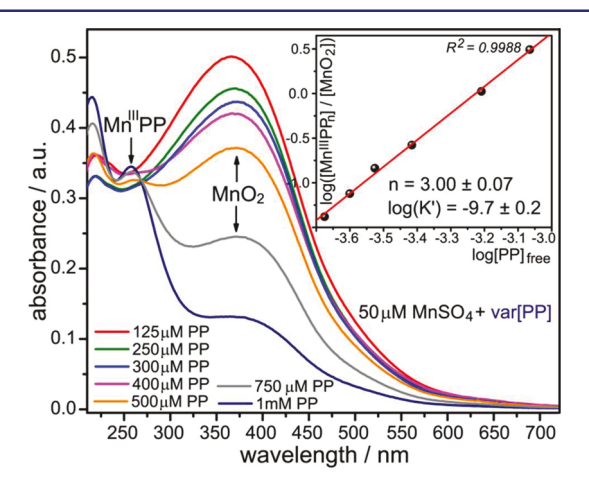


Figure 8. Spectra taken at the end of Mnx-catalyzed oxidation of 50 μM MnSO₄ in 10 mM NaPi buffer, pH 7.8, in the presence of the indicated amounts of NaPP. Increasing the amount of NaPP lowers the MnO₂ yield. Inset: [Mn^{III}PP]:[MnO₂] ratio evaluated from the final equilibrium spectra (Table S1) plotted versus free [PP] on log scale, from which the number of PP ligands, n = 3, and a conditional equilibrium constant, K', can be determined.

S2), where unconverted Mn(III) can still be observed at the end of the reaction. Evidently PP lowers the Mn(III) free energy sufficiently that the reaction does not go to completion. The dependence on PP concentration is consistent with establishment of a Mn(III)/MnO₂ equilibrium,

$$Mn^{III}(PP)_n + \frac{1}{2}O_2 + H_2O \rightarrow MnO_2 + nPP + 2H^+$$

$$K = \frac{[PP]^{n}[MnO_{2}][H^{+}]^{2}}{[Mn^{III}PP_{n}][P_{O_{2}}]^{1/2}}$$
(9)

Converting absorbances to concentrations (see Table S1), we plotted the log of the [MnIIIPP]:[MnO2] ratio against log[PP] (obtained by subtracting the bound PP from the formal PP concentration) to determine the conditional equilibrium constant,

$$\log K' = \log K + 2pH + \log[P_{O_2}]^{1/2}$$
(pH 7.8, $P_{O_2} = 0.2$ atm) (10)

and the number of PP ligands, from the rearranged equilibrium expression,

$$\log K' + \log \frac{[\mathrm{Mn^{III}PP_n}]}{[\mathrm{MnO_2}]} = n \log [\mathrm{PP}]$$
(11)

The excellent fit of the data to a straight line with integral slope (Figure 8, inset) validates the equilibrium model, and the

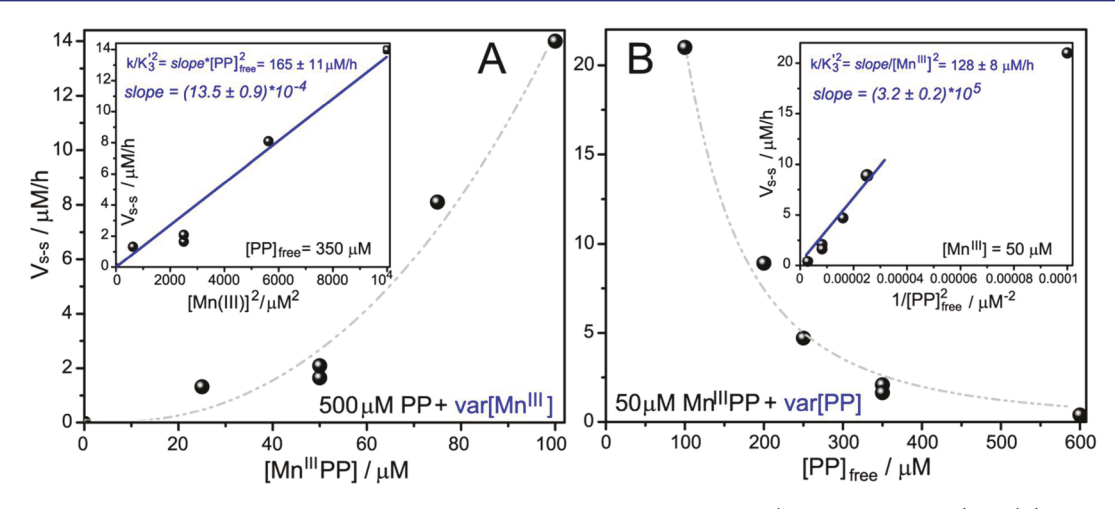


Figure 9. Dependence of the steady-state rate of MnO₂ production for 50 nM as-isolated Mnx (NaPi buffer, pH 7.8) on (A) the starting Mn(III) concentration in 0.5 mM NaPP and (B) the PP concentration, for 50 µM starting Mn(III). The steady-state rates were obtained from the linear portion of MnO₂ production curves, during early times when abiotic Mn(III) disproportionation was insignificant, Figures S5 and S10. [PP]_{free} was obtained by subtracting Mn(III)-complexed [PP] (=3[Mn(PP)₃) from the total [PP].

slope, n = 3, is consistent with literature reports that $Mn(III)(PP)_3$ species do form in the neutral pH range. 46,60-63

When Mn(IV) is produced from exogenous Mn(III), two Mn(III) bind simultaneously, since the steady-state rates, obtained from the linear portion of the Mn(IV) time courses (Figure S10), show a clear second-order dependence (Figure 9A).⁶⁴

The Mn(IV) turnover rate decreases with increasing PP concentration (Figure 9B), again reflecting solution chelation, this time of Mn(III). The dependence is second order, indicating that one PP is lost upon binding of each of the two Mn(III) to the enzyme. Since the dominant solution species is Mn(III)(PP)3, as demonstrated above, the loss of only one PP implies that the enzyme binds two Mn(III)(PP)₂ species, perhaps in a transient complex at the protein surface, as has been observed for transferrin when it is loaded by Fe(III) chelates. 65-67 Mn(III) would then transfer to the binuclear $Mn(III)(\mu-OH)_2Mn(III)$ site. Whether any PP remains bound at this stage is uncertain.

The second order rate dependencies for both Mn(III) and PP can be fit with a model,

rate =
$$k[Mn(III)(PP)_2]^2 = k\left(\frac{[Mn(III)(PP)_3]}{K_3'[PP]}\right)^2$$
 (12)

where k is the second-order rate constant (at the 50 nM Mnx concentration), and K'_3 is the third stepwise conditional (pH 7.8) formation constant for Mn(III)(PP)₃. Since our data on the Mn(III)/MnO₂ equilibrium (above) show that essentially all the Mn(III) in solution is present as Mn(III)(PP)3, the plot of rates vs [Mn(III)]² (Figure 9A, inset) and vs [PP]⁻² (Figure 9B, inset) should have respective slopes of

$$\frac{k}{(K_3')^2} \left(\frac{1}{[PP]^2}\right)$$

when $[PP]_{free} = 0.35 \text{ mM}$ and

$$\frac{k}{(K_3')^2}[Mn^{III}PP_3]^2$$

when [Mn(III)] = 0.05 mM). The Figure 9 insets show that the two slopes yield similar values of $\frac{k}{(K_3')^2} \approx 150 \ \mu\text{M/h}$. If K_3' were known, one could determine k, but a value for it has not been reported, as far as we are aware.

CONCLUSIONS

A central finding of this study is that, while Mnx catalyzes the oxidation of both Mn(II) and Mn(III) to MnO2, Mn(III) is incapable of direct electron transfer to the enzyme, and requires the presence of Mn(II) for reaction. Moreover, the reaction of Mn(III) is bimolecular, implying that Mn(III) binds at a binuclear site. These findings dovetail with our companion study, showing that Mnx requires activation, likely to form a low Mn(III)/Mn(II) reduction potential binuclear hydroxidebridged Mn(II) substrate, which reacts to form a binuclear dihydroxide-bridged Mn(III) intermediate. Since direct electron transfer is precluded, Mn(III) must be oxidized indirectly, via disproportionation and Mn(II) recycling, an inference supported by the evidence that the $Mn(III) \rightarrow Mn(IV)$ conversion step is slowed by PP chelation of the recycled Mn(II). Disproportionation can occur in the binuclear Mn(III) intermediate, or in a tetranuclear intermediate formed after a second turnover. The latter pathway is more likely since it leads directly to a binuclear oxo-bridged Mn(IV) product, without the need to stabilize a transient mononuclear Mn(IV) species. This product can readily condense into MnO₂, possibly after transport to a nucleation site.

Thus, the apparently difficult two-electron conversion of Mn(II) to MnO₂ does not require modification of the multicopper mechanism that MCOs use efficiently to harness O₂ and perform single electron transfers. Instead, MCO manganese oxidases can exploit the polynuclear chemistry of manganese and the ability of hydroxide- and oxo-bridges to stabilize the Mn(III) and Mn(IV) oxidation states.

Pyrophosphate, used in this study to trap and monitor Mn(III), does not alter the mechanism, but has multiple effects on the enzyme reaction. It slows the reaction by chelating both Mn(II) and Mn(III) in solution, and is also a strong inhibitor of activation, likely binding at or near the active site. Inhibition of the activation step may involve suppression of Mn(II)-bound water deprotonation, which is essential for activation, or of the accompanying conformation change that increases the Mn(II) affinity.

These chelate effects may play a role in modulating Mn biomineralization in nature. There are many bacterially produced chelating agents, some of which are no doubt responsible for significant Mn(III) concentrations frequently encountered in a variety of environments. 69-73 As demonstrated with PP, MnO₂ formation can be suppressed altogether at sufficiently high chelator concentrations. A case in point is the finding that MnO₂ formation is suppressed in P. putida GB-1, under conditions of iron limitation, due to the expression of the siderophore pyoverdine, which has a stronger affinity for Mn(III) than for Fe(III).^{74–76}

ASSOCIATED CONTENT

Supporting Information

The Supporting Information is available free of charge on the ACS Publications website at DOI: 10.1021/jacs.7b02772.

Experiments describing interference of HEPES buffer in Mnx assays with pyrophosphate; method to convert absorbances to MnO₂ and Mn(III)PP time-dependent concentrations; tabulated Mn(III)PP and MnO₂ equilibrium concentrations at the end of the pyrophosphate concentration-dependence experiment; Mn(III)PP and MnO₂ time courses obtained during Mnx-catalyzed oxidation of Mn(II) or Mn(III)PP substrates under different conditions; collections of the fitted [Mn(III)-PP] and [MnO₂] time courses obtained with as-isolated and pre-activated Mnx, and the extracted parameters used to plot [Mn(II)]-, [Mn(III)]-, and [PP] dependencies in the main text; and detailed descriptions and results of the abiotic, Mnx-pre-activation, and Mn(II)spiking experiments (PDF)

AUTHOR INFORMATION

Corresponding Author

*spiro@chem.washington.edu

ORCID 0

Alexandra V. Soldatova: 0000-0003-2876-6262 William H. Casey: 0000-0002-3275-6465 R. David Britt: 0000-0003-0889-8436

Author Contributions

[‡]C.A.R. and L.T. contributed equally to this work.

Notes

The authors declare no competing financial interest.

ACKNOWLEDGMENTS

This work was supported by the National Science Foundation: award numbers CHE-1410353 to T.G.S., CHE-1410688 to B.M.T., EAR-1231322 to W.H.C., CHE-1213699 and CHE-1665455 to R.D.B., and an NSF Postdoctoral Research Fellowship in Biology Award ID DBI-1202859 to C.A.R.

REFERENCES

- (1) Solomon, E. I.; Sundaram, U. M.; Machonkin, T. E. Chem. Rev. 1996, 96, 2563-2605.
- (2) Kosman, D. J. J. Biol. Inorg. Chem. 2010, 15, 15-28.
- (3) Solomon, E. I.; Augustine, A. J.; Yoon, J. Dalton Trans. 2008, 3921-3932.
- (4) Sakurai, T.; Kataoka, K. Cell. Mol. Life Sci. 2007, 64, 2642-2656.
- (5) Jones, S. M.; Solomon, E. I. Cell. Mol. Life Sci. 2015, 72, 869–883.
- (6) Machonkin, T. E.; Quintanar, L.; Palmer, A. E.; Hassett, R.; Severance, S.; Kosman, D. J.; Solomon, E. I. J. Am. Chem. Soc. 2001, 123, 5507-5517.

- (7) Solomon, E. I.; Kjaergaard, C. H.; Heppner, D. E. In Electrochemical Processes in Biological Systems; Lewenstam, A., Gorton, L., Eds.; Wiley: Hoboken, NJ, 2015.
- (8) Soldatova, A. V.; Tao, L.; Romano, C. A.; Stich, T. A.; Casey, W. H.; Britt, R. D.; Tebo, B. M.; Spiro, T. G. J. Am. Chem. Soc. 2017, DOI: 10.1021/jacs.7b02771, (preceding paper in this issue).
- (9) Butterfield, C. N.; Soldatova, A. V.; Lee, S.-W.; Spiro, T. G.; Tebo, B. M. Proc. Natl. Acad. Sci. U. S. A. 2013, 110, 11731-11735.
- (10) Butterfield, C. N.; Tebo, B. M. Metallomics 2017, 9, 183-191.
- (11) Butterfield, C. N.; Tao, L.; Chacón, K. N.; Spiro, T. G.; Blackburn, N. J.; Casey, W. H.; Britt, R. D.; Tebo, B. M. Biochim. Biophys. Acta, Proteins Proteomics 2015, 1854, 1853-1859.
- (12) Tao, L.; Stich, T. A.; Butterfield, C. N.; Romano, C.; Spiro, T. G.; Tebo, B. M.; Casey, W. H.; Britt, R. D. J. Am. Chem. Soc. 2015, 137, 10563-10575.
- (13) Tao, L.; Stich, T. A.; Liou, S.-H.; Soldatova, A. V.; Delgadillo, D. A.; Romano, C. A.; Spiro, T. G.; Goodin, D. B.; Tebo, B. M.; Casey, W. H.; Britt, R. D. J. Am. Chem. Soc. 2017, 139, 8868-8877.
- (14) Manchanda, R.; Brudvig, G. W.; Crabtree, R. H. Coord. Chem. Rev. 1995, 144, 1-38.
- (15) Mukhopadhyay, S.; Mandal, S. K.; Bhaduri, S.; Armstrong, W. H. Chem. Rev. 2004, 104, 3981-4026.
- (16) McEvoy, J. P.; Brudvig, G. W. Chem. Rev. 2006, 106, 4455-4483.
- (17) Yano, J.; Yachandra, V. Chem. Rev. 2014, 114, 4175-4205.
- (18) Whittaker, J. W. Arch. Biochem. Biophys. 2012, 525, 111-120.
- (19) Wu, A. J.; Penner-Hahn, J. E.; Pecoraro, V. L. Chem. Rev. 2004, 104, 903-938.
- (20) Waldo, G. S.; Penner-Hahn, J. E. Biochemistry 1995, 34, 1507-1512.
- (21) Khangulov, S. V.; Barynin, V. V.; Voevodskaya, N. V.; Grebenko, A. I. Biochim. Biophys. Acta, Bioenerg. 1990, 1020, 305-310.
- (22) Webb, S. M.; Dick, G. J.; Bargar, J. R.; Tebo, B. M. Proc. Natl. Acad. Sci. U. S. A. 2005, 102, 5558-5563.
- (23) Soldatova, A. V.; Butterfield, C. N.; Oyerinde, O. F.; Tebo, B. M.; Spiro, T. G. J. Biol. Inorg. Chem. 2012, 17, 1151-1158.
- (24) Kostka, J. E.; Luther, G. W.; Nealson, K. H. Geochim. Cosmochim. Acta 1995, 59, 885-894.
- (25) Kostka, J.; Nealson, K. H. In Techniques in microbial ecology; Burlage, R. S., Atlas, R., Stahl, D., Geesey, G., Sayler, G., Eds.; Oxford University Press: New York, 1998; p 58-78.
- (26) Perez-Benito, J. F.; Arias, C. J. Colloid Interface Sci. 1992, 152,
- (27) Siebecker, M.; Madison, A. S.; Luther, G. W., III Aquat. Geochem. 2015, 21, 143-158.
- (28) Hegetschweiler, K.; Saltman, P. Inorg. Chem. 1986, 25, 107-
- (29) Grady, J. K.; Chasteen, N. D.; Harris, D. C. Anal. Biochem. 1988, 173, 111-115.
- (30) Elzinga, E. J.; Kustka, A. B. Environ. Sci. Technol. 2015, 49, 4310-4316.
- (31) Ferreira, C. M. H.; Pinto, I. S. S.; Soares, E. V.; Soares, H. V. M RSC Adv. 2015, 5, 30989-31003.
- (32) Frieden, C. J. Biol. Chem. 1970, 245, 5788-5799.
- (33) Segel, I. H. Enzyme kinetics: Behavior and Analysis of Rapid Equilibrium and Steady-State Enzyme Systems; Wiley-Interscience: New York, 1993.
- (34) Synthetic MnO₂ colloids were prepared by the stoichiometric reduction of potassium permanganate (KMnO₄) with sodium thiosulfate (Na₂S₂O₃), following the method of Perez-Benito.
- (35) Perez-Benito, J.; Arias, C.; Amat, E. J. Colloid Interface Sci. 1996, 177, 288-297.
- (36) Campbell, K. A.; Force, D. A.; Nixon, P. J.; Dole, F.; Diner, B. A.; Britt, R. D. J. Am. Chem. Soc. 2000, 122, 3754-3761.
- (37) Campbell, K. A.; Lashley, M. R.; Wyatt, J. K.; Nantz, M. H.; Britt, R. D. J. Am. Chem. Soc. 2001, 123, 5710-5719.
- (38) Tyryshkin, A. M.; Watt, R. K.; Baranov, S. V.; Dasgupta, J.; Hendrich, M. P.; Dismukes, G. C. Biochemistry 2006, 45, 12876-12889.

- (39) Stich, T. A.; Lahiri, S.; Yeagle, G.; Dicus, M.; Brynda, M.; Gunn, A.; Aznar, C.; DeRose, V. J.; Britt, R. D. Appl. Magn. Reson. 2007, 31, 321
- (40) Reed, G. H.; Markham, G. D. In *Biological Magnetic Resonance*; Berliner, L. J., Ed.; Plenum Press: New York, 1984; Vol. 6, pp 73–142.
- (41) Mathur, P.; Crowder, M.; Dismukes, G. C. J. Am. Chem. Soc. 1987, 109, 5227-5233.
- (42) Pierce, B. S.; Elgren, T. E.; Hendrich, M. P. J. Am. Chem. Soc. **2003**, 125, 8748-8759.
- (43) Hayden, J. A.; Hendrich, M. P. J. Biol. Inorg. Chem. 2010, 15, 729-736.
- (44) Cooperman, B. S.; Mark, D. H. Biochim. Biophys. Acta, Gen. Subj. 1971, 252, 221–234.
- (45) Hyafil, F.; Blanquet, S. Eur. J. Biochem. 1977, 74, 481-493.
- (46) Watters, J. I.; Kolthoff, I. M. J. Am. Chem. Soc. 1948, 70, 2455—2460.
- (47) Martell, A. E.; Sillen, L. G. Stability Constants of Metal-Ion Complexes; The Chemical Society, Burlington House, London, 1964; p 190.
- (48) Smith, R. M.; Martell, A. E. In NIST critically selected stability constants of metal complexes database, Version 8.0; National Institute of Standards and Technology: Gaithersburg, MD, 2004.
- (49) Whittaker, M. M.; Pan, H.-Y.; Yukl, E. T.; Whittaker, J. W. J. Biol. Chem. **2007**, 282, 7011–7023.
- (50) Dube, C. E.; Wright, D. W.; Pal, S.; Bonitatebus, P. J.; Armstrong, W. H. J. Am. Chem. Soc. 1998, 120, 3704–3716.
- (51) Ruettinger, W. F.; Campana, C.; Dismukes, G. C. J. Am. Chem. Soc. 1997, 119, 6670–6671.
- (52) Chen, H.; Faller, J. W.; Crabtree, R. H.; Brudvig, G. W. J. Am. Chem. Soc. 2004, 126, 7345–7349.
- (53) Dismukes, G. C.; Brimblecombe, R.; Felton, G. A. N.; Pryadun, R. S.; Sheats, J. E.; Spiccia, L.; Swiegers, G. F. Acc. Chem. Res. 2009, 42, 1935–1943.
- (54) Mukherjee, S.; Stull, J. A.; Yano, J.; Stamatatos, T. C.; Pringouri, K.; Stich, T. A.; Abboud, K. A.; Britt, R. D.; Yachandra, V. K.; Christou, G. Proc. Natl. Acad. Sci. U. S. A. 2012, 109, 2257–2262.
- (55) Theil, E. C. Inorg. Chem. 2013, 52, 12223-12233.
- (56) Honarmand Ebrahimi, K.; Hagedoorn, P. L.; Hagen, W. R. Chem. Rev. 2015, 115, 295–326.
- (57) Romano, C. A.; Zhou, M.; Song, Y.; Wysocki, V.; Dohnalkova, A. C.; Kovarik, L.; Paša-Tolić, L.; Tebo, B. M. *Nat. Commun.* **2017**, submitted.
- (58) Overall charges of the Mn complexes have been omitted, since the protein ligands (likely carboxylates and imidazole) are unknown.
- (59) To investigate this equilibrium further, we monitored the reverse reaction when synthetic MnO_2 colloid (0.05 mM) was mixed with 2 mM PP (at this concentration, the Mnx-catalyzed forward reaction reaches ~5% completion). Absorption signal decreased for MnO_2 and increased for $Mn(III)(PP)_3$ slowly but steadily; the MnO_2 signal diminished by ~10% in 30 h and ~20% in 90 h. Addition of Mnx increased the rate to a small but detectable extent. Further work is needed to determine whether O_2 is actually produced.
- (60) Kolthoff, I. M.; Watters, J. I. Ind. Eng. Chem., Anal. Ed. 1943, 15, 8–13.
- (61) Bozor, I.; Simándi, L. I. J. Chem. Soc., Dalton Trans. 2002, 3226–3233
- (62) The lack of any curvature in the log plot indicates that the concentration of complexes with fewer than three PPs is negligible. PP stability constant data for Mn(III) are unavailable for neutral pH conditions, but for the similarly charged Ni(III)PP $_3$ at pH 7, an apparent stability constant of $10^{29.6}$ has been reported. This high value supports the conclusion that Mn(III)(PP) $_3$ dissociation is negligible at pH 7.8.
- (63) Ittah, E.; Shamir, D.; Zilbermann, I.; Maimon, E.; Yardeni, G.; Shames, A. I.; Meyerstein, D. *Inorg. Chim. Acta* **2013**, 405, 72–76.
- (64) Similar results were obtained whether as-isolated (Figure 9A) or pre-activated (Figure S17) enzyme was used.
- (65) Bates, G. W.; Billups, C.; Saltman, P. J. Biol. Chem. 1967, 242, 2810–2815.

- (66) Bates, G. W.; Billups, C.; Saltman, P. J. Biol. Chem. 1967, 242, 2816–2821.
- (67) Cheuk, M. S.; Loh, T. T.; Hui, Y. V.; Keung, W. M. J. Inorg. Biochem. 1987, 29, 301–311.
- (68) The Mn(III) concentration dependence with 0.5 mM PP and pre-activated enzyme was analyzed similarly (Figure S16 and Figure S17), giving $k/(K_3')^2$ almost 6 times the 150 μ M/h value obtained with as-isolated Mnx in 0.5 mM PP, consistent with the diminished PP effect on $V_{\rm max}$ suppression noted above for pre-activated enzyme with Mn(II) substrate.
- (69) Trouwborst, R. E.; Clement, B. G.; Tebo, B. M.; Glazer, B. T.; Luther, G. W., III. Science 2006, 313, 1955–1957.
- (70) Yakushev, E. V.; Pollehne, F.; Jost, G.; Kuznetsov, I.; Schneider, B.; Umlauf, L. Mar. Chem. 2007, 107, 388-410.
- (71) Madison, A. S.; Tebo, B. M.; Mucci, A.; Sundby, B.; Luther, G. W., III *Science* **2013**, *341*, 875–878.
- (72) Oldham, V. E.; Owings, S. M.; Jones, M. R.; Tebo, B. M.; Luther, G. W., III *Mar. Chem.* **2015**, *171*, 58–66.
- (73) Oldham, V. E.; Mucci, A.; Tebo, B. M.; Luther, G. W., III. Geochim. Cosmochim. Acta 2017, 199, 238–246.
- (74) Parker, D. L.; Sposito, G.; Tebo, B. M. Geochim. Cosmochim. Acta 2004, 68, 4809-4820.
- (75) Parker, D. L.; Morita, T.; Mozafarzadeh, M. L.; Verity, R.; McCarthy, J. K.; Tebo, B. M. Geochim. Cosmochim. Acta 2007, 71, 5672–5683.
- (76) Lee, S.-W.; Parker, D. L.; Geszvain, K.; Tebo, B. M. Front. *Microbiol.* **2014**, *5*, 301.